Electronic structure of palladium in the presence of many-body effects

A. Östlin,[1] W. H. Appelt,[1,2] I. Di Marco,[3] W. Sun,[3] M. Radonjić,[1,4] M. Sekania,[1,5] L. Vitos,[3,6,7]
O. Tjernberg,[8] and L. Chioncel[1,2]

[1]*Theoretical Physics III, Center for Electronic Correlations and Magnetism, Institute of Physics, University of Augsburg,
D-86135 Augsburg, Germany*
[2]*Augsburg Center for Innovative Technologies, University of Augsburg, D-86135 Augsburg, Germany*
[3]*Department of Physics and Astronomy, Division of Materials Theory, Uppsala University, Box 516, SE-75120 Uppsala, Sweden*
[4]*Scientific Computing Laboratory, Institute of Physics Belgrade, University of Belgrade, Pregrevica 118, 11080 Belgrade, Serbia*
[5]*Andronikashvili Institute of Physics, Tamarashvili 6, 0177 Tbilisi, Georgia*
[6]*Department of Materials Science and Engineering, Applied Materials Physics, KTH Royal Institute of Technology,
SE-10044 Stockholm, Sweden*
[7]*Research Institute for Solid State Physics and Optics, Wigner Research Center for Physics, P.O. Box 49, H-1525 Budapest, Hungary*
[8]*Materials Physics, KTH Royal Institute of Technology, SE-16440 Kista, Sweden*

Including on-site electronic interactions described by the multiorbital Hubbard model we study the correlation effects in the electronic structure of bulk palladium. We use a combined density functional and dynamical mean-field theory, LDA+DMFT, based on the fluctuation exchange approximation. The agreement between the experimentally determined and the theoretical lattice constant and bulk modulus is improved when correlation effects are included. It is found that correlations modify the Fermi surface around the neck at the *L* point while the Fermi surface tube structures show little correlation effects. At the same time we discuss the possibility of satellite formation in the high-energy binding region. Spectral functions obtained within the LDA+DMFT and *GW* methods are compared to discuss nonlocal correlation effects. For relatively weak local Coulomb interaction and Hund's exchange coupling the LDA+DMFT spectra show no major difference in comparison to *GW*.

I. INTRODUCTION

Transition metals have their density of states characterized by a partially filled narrow *d* band, superimposed on a broad free-electron-like *sp* band. The shape of the *d* band especially in the 3*d* series is a consequence of the construction of the *d* orbitals, as they overlap only to a limited extent with orbitals on neighboring atoms and consequently the hopping integrals between *d* orbitals are small, as is the bandwidth. This points towards the importance of short-range strong Coulomb repulsion for the 3*d* elements. An additional ingredient in the 3*d* series is the appearance of magnetism. In a partially filled shell of a free atom the exchange interaction between electrons favors the parallel alignment of electron spins (Hund's rule). In solids, electrons of the extended states and orbitals experience the competition between the kinetic energy favoring no spin alignment and the exchange interaction favoring spin alignment. If the band is narrow the energy gain from the exchange interaction may win and the spin alignment is favored. In this sense, the occurrence of magnetism in the 3*d* series is a consequence of the narrowness of the 3*d* band. A quantitative theory to explain the electronic structure and hence the physical properties of 3*d* elements has been consistently developed during the past decades in the form of the combined density functional theory (DFT) and dynamical mean-field theory (DMFT) [1–4], which is generally referred to as the LDA+DMFT method [4,5] (where LDA stands for local density approximation). In the LDA+DMFT scheme the LDA provides the *ab initio* material-dependent input (orbitals and hopping parameters), while the DMFT solves the many-body problem for the local interactions. Therefore, the LDA+DMFT approach is

able to compute, and even predict, properties of correlated materials. Theoretical results obtained with LDA+DMFT can be compared with experimental data obtained, for example, by photoemission spectroscopy (PES) [6,7]. In particular, this technique measures spectral functions, i.e., the imaginary part of the one-particle Green's function, and thus determines correlation-induced shifts of the spectral weight. Indeed, most experimental investigations on the electronic structure of the 3*d* metal Ni rely on PES [8,9]. Braun *et al.* [10] demonstrated the importance of local correlations in Ni by exploiting the magnetic circular dichroism in bulk sensitive soft x-ray PES measurements. One of the dominant correlation effects observed in the PES data for Ni is the satellite peak situated at 6 eV below the Fermi level [11–13]. This feature is not captured by LDA, but it is well explained by LDA+DMFT [12]. LDA+DMFT also reproduces the correct width of the occupied 3*d* bands and the exchange splitting [11,12,14].

As LDA+DMFT is very successful for 3*d* elements, this motivates us to investigate the applicability of LDA+DMFT to 4*d* transition-metal elements. Transition metals from the 4*d* series have larger bandwidths compared to that of the 3*d* elements and correspondingly larger kinetic energies, which will favor an itinerant bandlike picture over an atomiclike localized picture and somewhat weaker correlation effects. In our present study we focus on the 4*d* metal palladium. Despite being in the same group as Ni in the periodic table, the physical properties of Pd are very different, so a theoretical study including local and nonlocal correlation effects is particularly desirable. The electronic structure of Pd has been widely studied, both from a fundamental physics points of view and in its industrial applications as catalysts and hydrogen storage. As a late 4*d* transition-metal element, Pd is not far

from the ferromagnetic instability: it has a high density of states at the Fermi level and a large Stoner enhancement in the magnetic susceptibility [15]. On expansion (for a larger lattice constant) Pd turns ferromagnetic, as shown by DFT calculations [16]. Experimental studies involving PES have been used in the search for signatures of electronic correlations in Pd such as the existence of satellites in the spectral function [17,18]. Liebsch [19,20] investigated the satellite formation mechanism in detail using many-body methods, pointing out the importance of taking electron-hole and hole-hole scattering into account by ladderlike summations in the T-matrix formulation. Mårtensson and Johansson predicted a satellite in PES for Pd [21] at 8 eV binding energy, which is in good agreement with later experimental findings (~ 8.5 eV) by Chandesris *et al.* [17]. The method employed in Ref. [21] was semiempirical, using thermodynamic input data. In this study we discuss the satellite formation in Pd using *ab inito* self-consistent state-of-the-art calculations as well.

Complementary information can be obtained from the analysis of the Fermi surface. Features of the Fermi surface can be experimentally probed by photoemission spectroscopy and de Haas–van Alphen (dHvA) measurements. The so-called Kohn anomalies [22] may appear in the phonon dispersion relations of metals, arising from virtual scattering of conduction electrons from state $\mathbf{k}$ to $\mathbf{k}'$ connected by nesting vectors $\mathbf{q}$. The appearance of a Kohn anomaly in Pd, however, is still debated [23,24]. Therefore, the determination of possible Fermi-surface nesting in Pd remains of high interest.

Palladium is perhaps the best studied high-susceptibility paramagnet and played an important role in elucidating several aspects of the theory of spin fluctuations. Among the elements, Pd is traditionally taken as the best candidate for observing spin fluctuations because of its high electronic density of states and large Stoner enhancement in the magnetic susceptibility. Specific heat experiments [25] showed a reduction in the electronic specific heat coefficient of 7% in a magnetic field of about 10 T, suggesting that strong spin fluctuations do appear in Pd. The reduction of spin-fluctuation contributions to the electronic specific heat at high magnetic fields is well established theoretically by several works: Doniach and Engelsberg [26], Berk and Schrieffer [27], Béal-Monod and co-authors [28,29], and many others. In their classical works, the Crabtree group experimentally investigated the evidence of spin fluctuations in Pd by measuring the cyclotron effective masses and the amplitude of the dHvA effect as a function of the magnetic field [30,31]. These typical measurements provide in principle information about spin-fluctuation contributions to the conduction electron properties. While the former allows one to obtain information about the density of states at the Fermi level, which determines the electronic specific heat, the latter measures the difference in volume between the spin-up and spin-down Fermi surfaces, which determines the magnetization. The absence of significant field dependence of the cyclotron effective mass and the spin splitting factor [30,31] implies that the spin-fluctuation contributions to the electronic specific heat and static spin susceptibility $\chi = M/H$ are not appreciably affected by applied fields up to 13 T. This is consistent with the theoretical estimations made by Brinkmann and Engelsberg [32] and Hertel *et al.* [33] that magnetic fields much larger than 13 T are required

to suppress the spin fluctuations in Pd. Highly accurate LDA calculations were performed to estimate the parameters entering in Moriya's spin-fluctuation theory [34]; in particular the Landau functional for Pd was used to connect critical fluctuations beyond the local density approximation with the band structure. The magnetic properties and dynamical fluctuations in Pd were discussed recently by Larson *et al.* [35]. It was pointed out [35] that the key parameter for the nontrivial properties of Pd is the mean-square amplitude of the spin fluctuations, which is a nonlocal quantity determined by the momentum-dependent spin susceptibility in a large part of the Brillouin zone, and therefore nonlocality is expected to play a significant role in the physical properties. It is one of the aims of this work to identify local and nonlocal correlation effects on the spectral function by comparing results obtained via LDA+DMFT and *GW* methods [36].

The results presented here include the electronic structure, the Fermi surface and nesting vectors of Pd, and the satellite formation in the high-binding-energy region of the density of states. Most of our results have been obtained within the full-potential linearized muffin-tin orbitals (FPLMTO) method implemented within the RSPt code [37], which has previously proven to be able to accurately determine ground-state quantities within LDA+DMFT for 3d transition metals [38,39]. Self-consistent quasiparticle *GW* calculations have also been performed [40,41], which allows us to discuss the effect of nonlocal electronic correlations in Pd. The paper is organized as follows: Section I is an introduction. In Sec. II we present computational methods and details of the calculations. Section III A presents the total-energy data, from which we extract the optimal U and J values matching the experimental and the calculated equilibrium lattice parameters. We also present results concerning the onset of ferromagnetic long-range order upon lattice expansion. In Sec. III C the calculated spectral function of palladium is shown, and the relation to the photoemission satellite is discussed in detail. The effect of nonlocal correlations is discussed in Sec. III D.

II. COMPUTATIONAL METHODS AND DETAILS

A. The LDA+DMFT method

Correlation effects in the valence Pd 4d orbitals were included via an on-site electron-electron interaction in the form $\frac{1}{2} \sum_{i\{m,\sigma\}} U_{mm'm''m'''} c^{\dagger}_{im\sigma} c^{\dagger}_{im'\sigma'} c_{im'''\sigma'} c_{im''\sigma}$. Here, $c_{im\sigma}$ ($c^{\dagger}_{im\sigma}$) annihilates (creates) an electron with spin σ on the orbital m at the lattice site i. The Coulomb matrix elements $U_{mm'm''m'''}$ are expressed in the usual way [42] in terms of Slater integrals. Since specific correlation effects are already included in the local spin-density approximation (LSDA), so-called "double-counted" terms must be subtracted. To take this into account, we employed the interpolation double-counting scheme [43]. For the impurity solver a fluctuation exchange (FLEX) [44] type of approximation was used for the multiorbital case [45–47]. In contrast to the original formulation of FLEX [44], the spin-polarized T-matrix FLEX (SPTFLEX) is employed for the present calculations, which treats the particle-particle and the particle-hole channel differently [45–47]. While the particle-particle processes are important for the renormalization of the effective interaction [48], the particle-hole channel

describes the interaction of electrons with the spin fluctuations, which represents one of the most relevant correlation effects in Pd. In addition, the advantage of this computational scheme lies in the treatment of the Coulomb matrix elements in a full spin and orbital rotationally invariant form, relevant for realistic materials.

B. The self-consistent quasiparticle *GW* method

In recent years, first-principles calculations involving the *GW* approximation [36] have become more popular. In particular *self-consistent GW* formulations are promising because they can more accurately calculate quantities like band gaps as compared to "one-shot" *GW* approaches [41]. In these methods, the first step is to compute the band structure of the solid, usually within DFT-LDA. The density response function is then calculated by the random-phase approximation (RPA) and employed to evaluate the dielectric function and the screened Coulomb interaction W. The matrix elements of the self-energy are added as corrections to the LDA eigenvalues, and the effective potential is self-consistently updated. In spite of the simplified formalism of calculation, as compared to that of the full *GW* scheme, a good agreement with experiment for several materials has been obtained [41]. In this study we employed the quasiparticle self-consistent *GW* (QSGW) method [40,41]. Our main object of interest is the self-energy-corrected eigenvalue for band n and Bloch vector $\mathbf{k}$,

$$E_{\mathbf{k}n} = \epsilon_{\mathbf{k}n} + Z_{\mathbf{k}n}\Delta\Sigma_{\mathbf{k}n}, \tag{1}$$

where the operator $\Delta\Sigma_{\mathbf{k}n} = \langle\Psi_{\mathbf{k}n}|\,\Sigma(\mathbf{r},\mathbf{r}',\epsilon_{\mathbf{k}n}) - V_{xc}(\mathbf{r})\,|\Psi_{\mathbf{k}n}\rangle$. The self-energy is given in terms of the Green's function and the screened Coulomb interaction W: $\Sigma(\mathbf{r},\mathbf{r}',\omega) = \frac{i}{2\pi}\int d\omega' G(\mathbf{r},\mathbf{r}',\omega - \omega')W(\mathbf{r},\mathbf{r}',\omega')e^{-\delta\omega'}$. From the slope of the real part one can obtain the renormalization factor

$$Z_{\mathbf{k}n} = \left[1 - \frac{\partial\mathrm{Re}\,\Sigma_{\mathbf{k}n}(\omega)}{\partial\omega}\right]^{-1}. \tag{2}$$

In a direct comparison with the LDA+DMFT results, *GW* calculations reveal if significant nonlocal correlation effects occur in Pd.

C. Technical details

The LDA+DMFT calculations were done using the FPLMTO code RSPt [37] as a base for the underlying density functional theory calculations. The RSPt calculations were based on the local-density approximation with the parametrization of Perdew and Wang [49] for the exchange-correlation functional. Three kinetic energy tails were used, with corresponding energies 0.3, −2.3, and −1.5 Ry. Palladium is a face-centered-cubic metal, and the **k**-mesh we used had the size $16 \times 16 \times 16$ for the equations of state, $24 \times 24 \times 24$ for the other calculations, and Fermi-Dirac smearing with $T = 400$ K (the same temperature as was used for the imaginary-frequency Matsubara mesh). The muffin-tin radius was set to 2.45 Bohr atomic units (a.u.) and was kept constant throughout all unit-cell volumes. For the charge density and potential angular decomposition, inside the muffin-tin spheres, a maximum angular momentum $l_{max} = 8$ was set. The calculations included spin-orbit coupling

and scalar-relativistic terms within the muffin-tin spheres, unless otherwise noted. The SPTFLEX impurity solver was implemented in the Matsubara domain, and we used 2048 imaginary frequencies and an electronic temperature of 400 K. The analytic continuations of the self-energy from imaginary frequencies to the real energy axis in the complex plane were performed by Padé approximants [50].

The QSGW scheme used in this study is implemented into the LMSuite package [40,41], which is based on the full-potential linear muffin-tin orbitals code by M. Methfessel *et al.* [51]. The muffin-tin radius was chosen to be 2.63 a.u, and the integration of the Brillouin zone (BZ) was mapped with $24 \times 24 \times 24$ **k**-points. For the *GW* calculation, we reduced the **k**-points to $6 \times 6 \times 6$ [41]. A double-κ basis set with $l_{max} = 4$ was used, including the semicore $4p$ states with local orbitals. This basis set allows for an accurate description of the high-lying conduction-band states. Spin-orbit coupling was included within the muffin-tin spheres.

We point out that both the RSPt and the QSGW methods employ the full-potential linearized muffin-tin orbital basis set, but using different implementations. As can be seen in Sec. III D, this causes no major differences between the RSPt and the QSGW LDA results.

III. RESULTS AND DISCUSSION

A. Equation of state

We begin our study by showing that LDA+DMFT can accurately determine the equilibrium lattice constant and bulk modulus, the two most important ground-state properties. The Coulomb and exchange parameters U and J used in the DMFT calculations are considered adjustable parameters in this study. In principle, they can be calculated from first principles too [52]. In this section we adjust the U and J values such that the calculated equation of state (EOS) energy-volume curve reproduces the experimental lattice constant (see Table I for a collection of experimental lattice constants from the literature).

In Fig. 1 (top), EOS curves for different values of U and J are presented. The experimental volume has been marked out. The equilibrium volume V_0 and bulk modulus B_0 for each of the curves can be seen in Table II. One

TABLE I. Experimental lattice constants a (and equivalent unit-cell volume) of palladium from various sources, as a function of temperature.

T (K)	a (Å)	a (a.u.)	Volume (a.u.^{3})	Ref.
853	3.9184	7.4047	101.50	[53]
673	3.9088	7.3866	100.76	[53]
297	3.9049	7.3792	100.45	[54]
296	3.8904	7.3518	99.34	[53]
296	3.8902	7.3514	99.32	[53]
120	3.8830	7.3378	98.77	[53]
23	3.8907	7.3524	99.36	[54]
0[a]	3.881	7.334	98.62	[55]
0[b]	3.877	7.326	98.32	[55]

[a]Estimated from room temperature using linear thermal expansion coefficient; see Ref. [55].

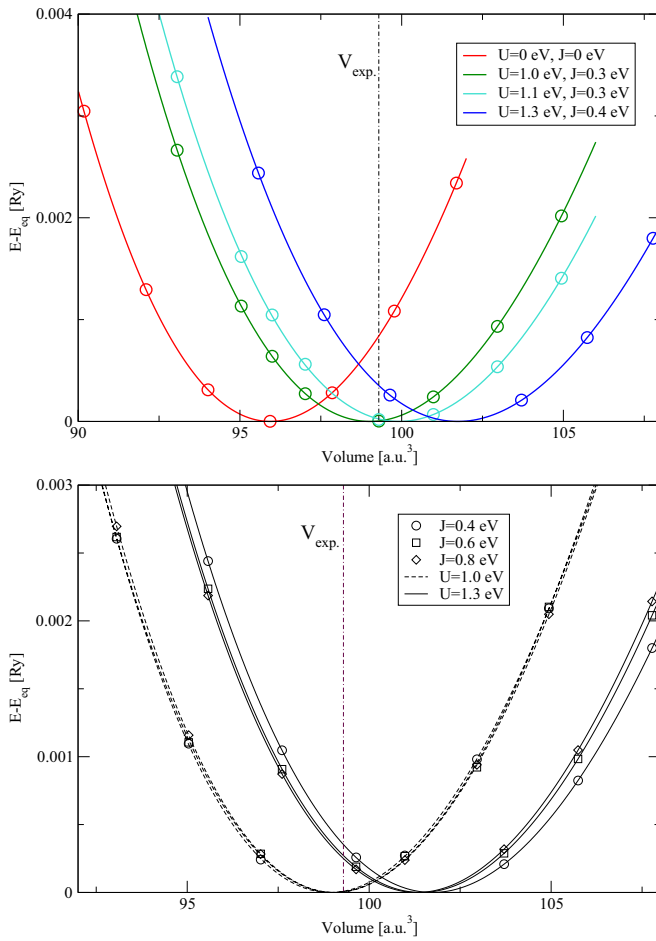[b]Corrected for zero-point anharmonic expansion; see Ref. [55].

FIG. 1. Equation of state curves. Top: Effect of increasing U. LDA (red) compared to $U = 1.0$ eV, $J = 0.3$ eV (green); $U = 1.1$ eV, $J = 0.3$ eV (turquoise); and $U = 1.3$ eV, $J = 0.4$ eV (blue). Bottom: Effect of altering J while keeping U fixed, for $U = 1.0$ eV (dashed line) and $U = 1.3$ eV (solid line).

TABLE II. Equilibrium volumes V_0 and bulk moduli B_0 extracted from equation-of-state fitting function (Birch-Murnaghan), for different sets of U and J parameters. The experimental volume 99.3 a.u.^{3} is taken from the room-temperature data of Ref. [53], which differs from the $T = 0$ K data by $<1\%$. The experimental bulk modulus is 189 GPa [56].

U (eV)	J (eV)	V_0 (a.u.^{3})	B_0 (GPa)
0	0	95.94	226.6
1.0	0.3	99.02	190.6
	0.4	98.92	192.2
	0.6	99.03	192.2
	0.8	99.05	193.2
1.1	0.3	99.92	181.7
1.3	0.4	101.74	167.7
	0.6	101.42	171.9
	0.8	101.31	174.7
3.0	0.3	127.91	122.3
	0.9	124.07	124.2

observes (Fig. 1, top) that $U = J = 0$ eV (red curve), i.e., the LDA, underestimates the volume, which is commonly known. The generalized gradient approximation (GGA) to the exchange-correlation potential, as pointed out for Pd in Ref. [57] (data not shown here), overestimates the lattice constant and leads to a ferromagnetic ground state and is therefore unsuitable. As the value of U is increased, the computed lattice constant approaches the experimental value from below. For $U = 1.0$ eV the calculated V_0 and B_0 for different exchange parameters J are given in Table II, and the values are closer to experiment than the LDA value. The effect of varying the exchange parameter J on the EOS can be observed in Fig. 1 (bottom, dashed lines). The equilibrium volumes are tabulated in Table II and give a standard deviation of 0.05 a.u.^{3}, which is of the same order as the scattering in the data for room temperature (see $T = 296$ K in Table I). At $U = 1.1$ eV and $J = 0.3$ eV, V_0 is overestimated compared to the experimental value, while B_0 is underestimated. Increasing U to 1.3 eV leads to an even larger V_0 and a smaller B_0. Varying J at this value of U gives a standard deviation of 0.18 a.u.^{3}, which is an order of magnitude larger than the standard deviation at $U = 1.0$ eV. The effect of exchange J on the volume is larger for $U = 1.3$ eV than for $U = 1.0$ eV, but it is still below the experimentally observed thermal expansion (see Table I). The increase of J (for a fixed $U = 1.3$ eV) decreases the equilibrium volume, which is opposite to the trend given by increasing U. However, this is a small effect and not relevant to this study. By increasing U even further to 3 eV, the same trend of increasing V_0 and decreasing B_0 is maintained (see Table II).

Based on the results presented in this section, $U = 1.0$ eV and $J = 0.3$ eV can be taken as a reasonable choice to reproduce the lattice constant and bulk modulus in our LDA+DMFT calculations.

B. Ferromagnetic instability

It is known that palladium is on the verge of ferromagnetism, having a large density of states at the Fermi level $D(E_F)$ leading to a large static susceptibility. An early theory that tried to explain the magnetic transition in itinerant electron systems was the Stoner model. According to this model, a magnetic state is favored over a nonmagnetic state when the criterion $D(E_F)I \geqslant 1$ is fulfilled, where I is the Stoner parameter [58]. This criterion points to the possibility of inducing magnetic order by increasing $D(E_F)$. In some cases, this can be achieved by reducing the effective dimensionality of the system. To create magnetic order, attempts have been made to lower the dimensionality of Pd systems, e.g., by creating nanoparticles and nanowires [59–61] or thin films [62]. There are also density functional theory studies that indicate that bulk palladium turns ferromagnetic as the volume is expanded [16,63–65].

In Fig. 2 the magnetic moment in units of μ_B is plotted as a function of lattice constant. For the LDA, within the scalar-relativistic approximation (red curve), a magnetic onset is brought about at a lattice constant of 7.65 a.u. This is about 4% larger than the experimental lattice constant, which is in accordance with previous studies, where the magnetic onset varies between a 1% and 6% increase of the lattice constant.
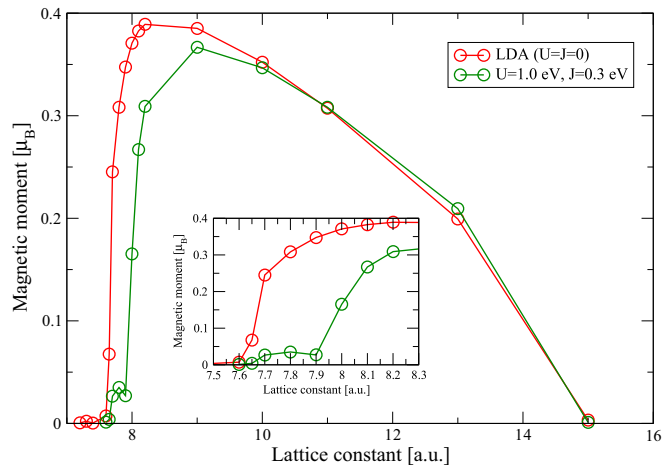
FIG. 2. Magnetic moment calculated as a function of volume, within the LDA (red circles) and within LDA+DMFT (green circles), for $U = 1.0$ eV and $J = 1.3$ eV. Relativistic effects were treated using the scalar-relativistic approximation.

Hong and Lee [65] point out that this variance could be due to the sensitivity of $D(E_F)$ on the **k**-point mesh and show that $D(E_F)$ is difficult to fully converge even at dense mesh sizes. Note that the curve reaches a maximum (about $0.4\mu_B$) and then decreases toward zero magnetic moment at large lattice constants. A full charge transfer to the d states has then been accomplished, leading to fully occupied d states with no net magnetic moment [16].

We next calculated the magnetic moment as a function of increasing lattice constant within the LDA+DMFT scheme, using the scalar-relativistic approximation, and setting $U = 1.0$ eV and $J = 0.3$ eV (Fig. 2, green curve). The magnetic transition is pushed further upwards in volume, compared to the scalar-relativistic LDA curve (red), giving a transition first into a "low-moment" and then into a "high-moment" state. We also note that the LDA+DMFT curve more or less coincides with the LDA curve at larger lattice constants. The system is then close to having a fully occupied d band, where correlation should have a negligible effect. Therefore, DMFT is able to capture some dynamical spin-fluctuation effects, and this could explain the suppression of the magnetic moment at those intermediate volumes, where the LDA still produces noticeable moments.

C. Density of states and Fermi surface

1. Spectral functions and the formation of satellite structure

The density of states (DOS) at the experimental lattice constant is presented in Fig. 3. Including electronic correlations, for increased values of the local Coulomb parameter U, in the higher-binding-energy region a satellite structure develops. We tuned J for fixed U and saw no significant change in DOS (not shown). Hence, the satellite position is mostly insensitive to the value of the exchange parameter J.

The quasiparticle weights $Z = (1 - \partial\mathrm{Re}[\Sigma(E)]/\partial E|_{E_F})^{-1}$ for the different U, shown in Fig. 3, are in the range $Z = 0.975-0.916$ for $U = 1-4$ eV. These correspond to effective mass ratios $m^*/m_{\mathrm{LDA}} = Z^{-1} = 1.03-1.09$, where m_{LDA} is the LDA band mass. This should be compared

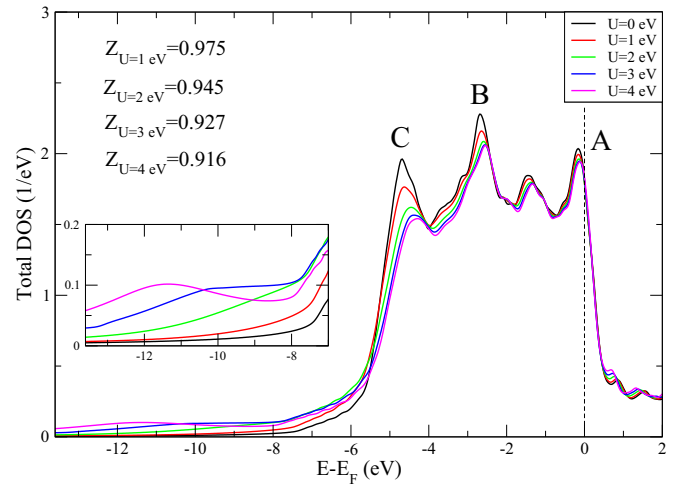FIG. 3. Total density of states as a function of the Coulomb interaction U. Note that the peak closest to the Fermi level (marked by A) is pinned and that the lowest-lying peak (C) decreases in intensity while a satellite structure is formed for high binding energies (see inset). Corresponding quasiparticle weights $Z = (1 - \partial\mathrm{Re}[\Sigma(E)]/\partial E|_{E_F})^{-1}$ are given in the upper left corner.

with $m^*_{\mathrm{sp.heat}}/m_{\mathrm{LDA}} = 1.66$, where $m^*_{\mathrm{sp.heat}}$ is estimated from electronic specific heat measurements and m_{LDA} is taken from band-structure calculations [66,67], which is considerably larger than what we obtain in this study. It should be noted that the electron-phonon coupling $\lambda_{e\text{-ph}}$ is not included in our self-energy, and previous theoretical studies have shown this quantity $\lambda_{e\text{-ph}}$ to be in the range 0.35–0.41 [68,69]. Recent angle-resolved PES (ARPES) by Hayashi *et al.* [67] estimated the electron-phonon coupling to be $\lambda_{e\text{-ph}} \approx 0.39$, and the electron-electron and electron-paramagnon coupling to be $\lambda_{e\text{-e}} + \lambda_{e\text{-para}} \approx 0.08$, leading to an effective mass $m^*_{\mathrm{ARPES}}/m_{\mathrm{LDA}} = 1 + \lambda_{\mathrm{tot}} \approx 1.5$. Using Hayashi *et al.*'s [67] value for $\lambda_{e\text{-ph}}$, together with our calculated self-energy, the effective mass is $m^*/m_{\mathrm{LDA}} = 1.42-1.48$, for $U = 1-4$ eV. This is in good agreement with Hayashi *et al.* [67], but still underestimates the value from specific heat measurements. It should be noted that our quasiparticle weights Z are averaged over the BZ, while Ref. [67] investigated specific paths in the BZ, being also a surface-sensitive study. The overall magnitude, however, is similar as this comparison shows.

Just below the Fermi level a dominant peak, with a relatively large value of the density of states, is situated with a maximum at about -0.15 eV (marked by A) for all investigated U values. A second major peak (B) is situated in the middle of the valence band around -2.7 eV at $U = 0$ and is shifted to approximately -2.5 eV as U is increased. The third major peak (C) is at the bottom of the d band near -4.7 eV and is shifted towards -4.4 eV as correlation is increased. The contributions of different bands to the peaks in the DOS can be inferred by studying the spectral function along high-symmetry lines in the BZ; see Fig. 4.

Concerning the high-energy binding region in the photoemission spectra, there exist discrepancies of the order of 0.5 eV between experiment and band-structure calculations, as pointed out by Kang *et al.* [70]. The LDA seems to overestimate the bandwidth of Pd as compared to the measured
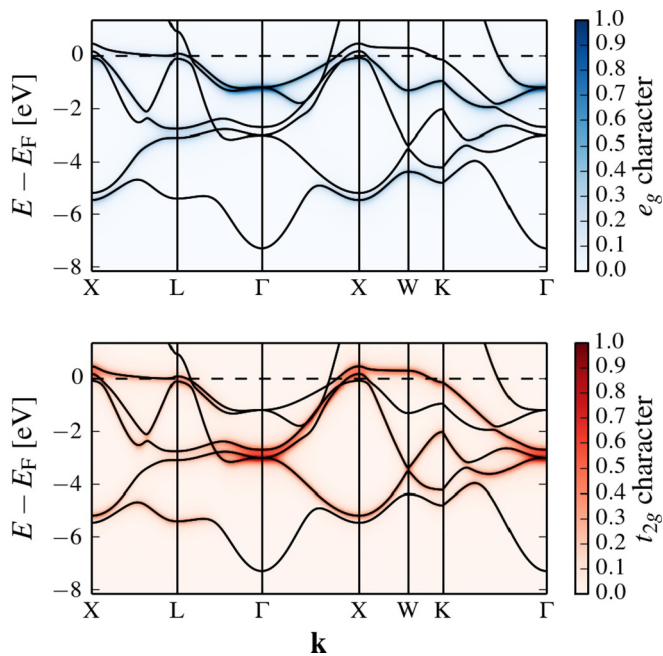
FIG. 4. LDA orbital-resolved spectral functions along high-symmetry lines in the BZ. Top: e_g symmetry. Bottom: t_{2g} symmetry.

PES bandwidth, and some experimental states are located closer to the Fermi level than the theoretical states [70–73]. It was proposed [70] that surface and correlation effects could modify the LDA band structure, explaining the discrepancies. It is not altogether clear how to separate these two effects from each other since both bulk and surface states will contribute to the PES, especially for low photon energies. Kang *et al.* [70] performed combined PES and LDA band-structure calculations for Pd, and their results indicate that the surface effects could indeed explain the bandwidth narrowing. However, they also ruled out many-body correlation effects since they found no trace of a satellite in the PES. The absence of the satellite might be caused by a missing $4p$-$4d$ photoabsorption threshold in Ref. [70], since the energy range (around 55 eV photon energy) does not seem to be investigated. The experimental photoemission studies in Refs. [17,18] scan this range and do indeed find a satellite. The $4p$-$4d$ photoabsorption process can be viewed as follows: A photon with energy at the $4p$ core level will excite a core electron to the Fermi level. As the $4p$ core hole is filled by a valence electron, the resulting valence hole will interact with the photoabsorbed electron and contribute to the satellite intensity. Note that the $4p$-$4d$ photoabsorption will affect the satellite intensity, but not its position [74]. The satellite position will be determined by the valence hole spectral function, which we access in our calculations. We cannot capture the contribution from the core levels on the spectra, and hence the satellite intensity which we obtain should not be directly compared with experiment. From comparison with Fig. 3 and the experimental satellite position 8.5 eV [17], the U value needed to reproduce the satellite position can be estimated to be between 2 and 3 eV. By including correlations we also get a shift of the B and C peaks to lower binding energy, in better agreement with experiment. The B peak position has been measured at −2.55 eV [72], −2.4 eV [18], and −2.5 eV (estimated from

Ref. [70]), which indicates that the LDA positions this peak at too-high binding energy (about −2.7 eV in this study) and that including correlations will improve the peak position in comparison with experiment. Here we emphasize that no attempt was made to model the surface states; instead only bulk calculations were performed. Note that matrix element effects were also not taken into account in this study.

As shown in Sec. III A U values above 1.0 eV overestimate the equilibrium lattice constant. Hence a different U value is required to match the experimental spectra than the one that reproduces the equilibrium volume. The same discrepancy was also encountered for Ni [38,75].

It is interesting to discuss the satellite formation in Pd, in comparison with Ni. The effect of electron correlations on energies of one-electron removal from a partially filled band is described in terms of interactions between three-body configurations, one hole plus one electron-hole pair, giving the rise to hole-hole and hole-electron scattering [19,20]. The effectiveness of these scattering processes depends not only on the strength of the screened on-site electron-electron interaction, but also on the occupation of orbitals involved in the scattering process. In particular on the number of empty d states, necessary for the creation of three-particle configurations, since no electron-hole pair can be added to a completely filled band, in the case of nickel where only the minority-spin band has a sizable number of empty states available, the creation of a majority-spin hole will be followed by scattering processes involving only opposite spin electron-hole pairs. The strength of the interaction for this channel is proportional to U, while the creation of a minority-spin hole will involve a scattering with parallel spin electron-hole pairs only of strength proportional to $U - J$. In Pd both spin channels are always symmetric (paramagnetic metal), while for Ni the exchange splitting redistributes holes in the d bands. Even for the reduced scattering amplitudes of electron-hole pairs, the T-matrix formalism generates a satellite structure, but due to the small satellite weight it is hardly discernible for valence-state spectroscopy.

2. Fermi surface

The Fermi surface of Pd was extensively studied within density functional theory formalism [66,76,77]. Here we present a detailed comparison of the Fermi surface obtained by different methods including correlation effects. In Fig. 5 (bottom left), we present a cut of the LDA Fermi surface in the $k_x - k_y$ plane together with a projection of the three-dimensional Fermi surface sheets (Fig. 5, top left). The Fermi surface geometry contains the closed electron surface around the Γ point, and a set of hole ellipsoids at the X points. Open hole surfaces consists of cylinders, extending in the [100] and [010] directions (i.e., along the X-W-X paths) and intersecting in pairs at the symmetry points X; see top right of Fig. 5. The open hole surfaces are particularly interesting as they are associated with the large effective masses and contribute substantially to the density of states near the Fermi level [77]. The Kohn anomaly [22], in the slope of the $[\xi\xi 0]$ transverse acoustic branch of the Pd phonon dispersion, is attributed to Fermi surface nesting between these open hole cylinders (see Ref. [23] and references therein). Previous calculations also predicted the existence of small L pockets, which were
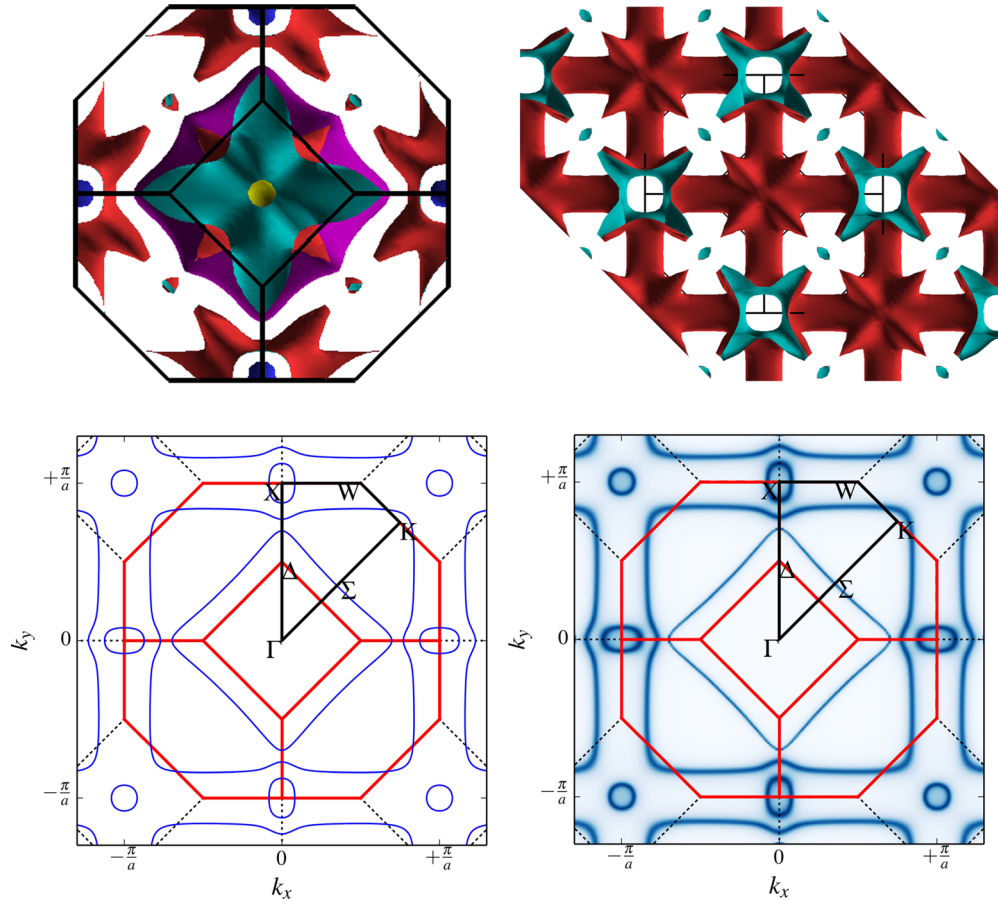
FIG. 5. Fermi surfaces. Top left: three-dimensional Fermi surface in the first BZ, projected on the k_x-k_y plane. Note the X hole pockets centered at the square faces (blue, hole side; yellow, electron side), the L hole pockets centered at the hexagonal faces (red, hole side; turquoise, electron side), and the tube hole structures intersecting at the X points (red, hole side; turquoise, electron side). Also note that the L pockets only exist if spin-orbit terms are included. A large electron surface sheet is centered around the Γ point (purple). Top right: Hole tube structure as seen in the extended zone scheme. Bottom left: Cut at $k_z = 0$ within the LDA. Bottom right: Cut at $k_z = 0$ within the LDA+DMFT, $U = 1.0$ eV and $J = 0.3$ eV. The three-dimensional Fermi surface was created with the XCrysden software [78].

seen if spin-orbit coupling was taken into account [66,76]. These L pockets were later confirmed by magnetoacoustic measurements [79].

The orbital character of the Fermi surface sheets can be determined by investigation of the orbital-resolved spectral function; see Fig. 4. The tube structure (stemming mostly from the flat band between the W and the X symmetry points) has mostly t_{2g} character, which was pointed out already by Kanamori [80]. The Fermi surface obtained with LDA+DMFT is also presented in Fig. 5 (bottom right). There is no significant difference between the Fermi surfaces from LDA and LDA+DMFT. The diameters of the tube structures are only weakly affected. The Fermi-surface nesting vector, believed to be responsible for the Kohn anomaly in the phonon dispersion of Pd, is estimated to be $\mathbf{q} = \frac{2\pi}{a}[0.30, 0.30, 0]$, in close agreement with previous studies [23]. Therefore, the Kohn anomaly is already well captured at the level of the LDA [23].

D. Local and nonlocal correlation effects

In order to investigate the effect of nonlocal electron correlations on the electronic structure of Pd, calculations employing the QSGW method were also performed. The band structure, the spectral functions, and the Fermi surfaces were calculated using the experimental volume.

In Fig. 6 (top left) the band structure along high-symmetry lines within the Brillouin zone is plotted. The bands within the LDA from RSPt (solid green lines) and from QSGW (dashed blue lines) coincide well. Turning on correlation effects, the bands are modified as compared to the LDA result. The QSGW (red dots) and the LDA+DMFT (blue energy scale) are nearly coinciding around the Fermi level, and differences are mainly visible at higher energies. Around the Γ point, for energies between -6 eV and the Fermi level, the QSGW bands are shifted towards the Fermi level to a larger extent than the LDA+DMFT bands. For binding energies larger than 6 eV, the lowest band is shifted downwards in energy to a larger extent than the LDA+DMFT bands. The trends (upwards or downwards shifts in energy) are, however, the same for both methods, indicating that the U value used in LDA+DMFT ($U = 1.0$ eV) is too small to reproduce the correct quasiparticle eigenvalue position. This was also found when LDA+DMFT spectral functions were compared with the experiment in Sec. III C.
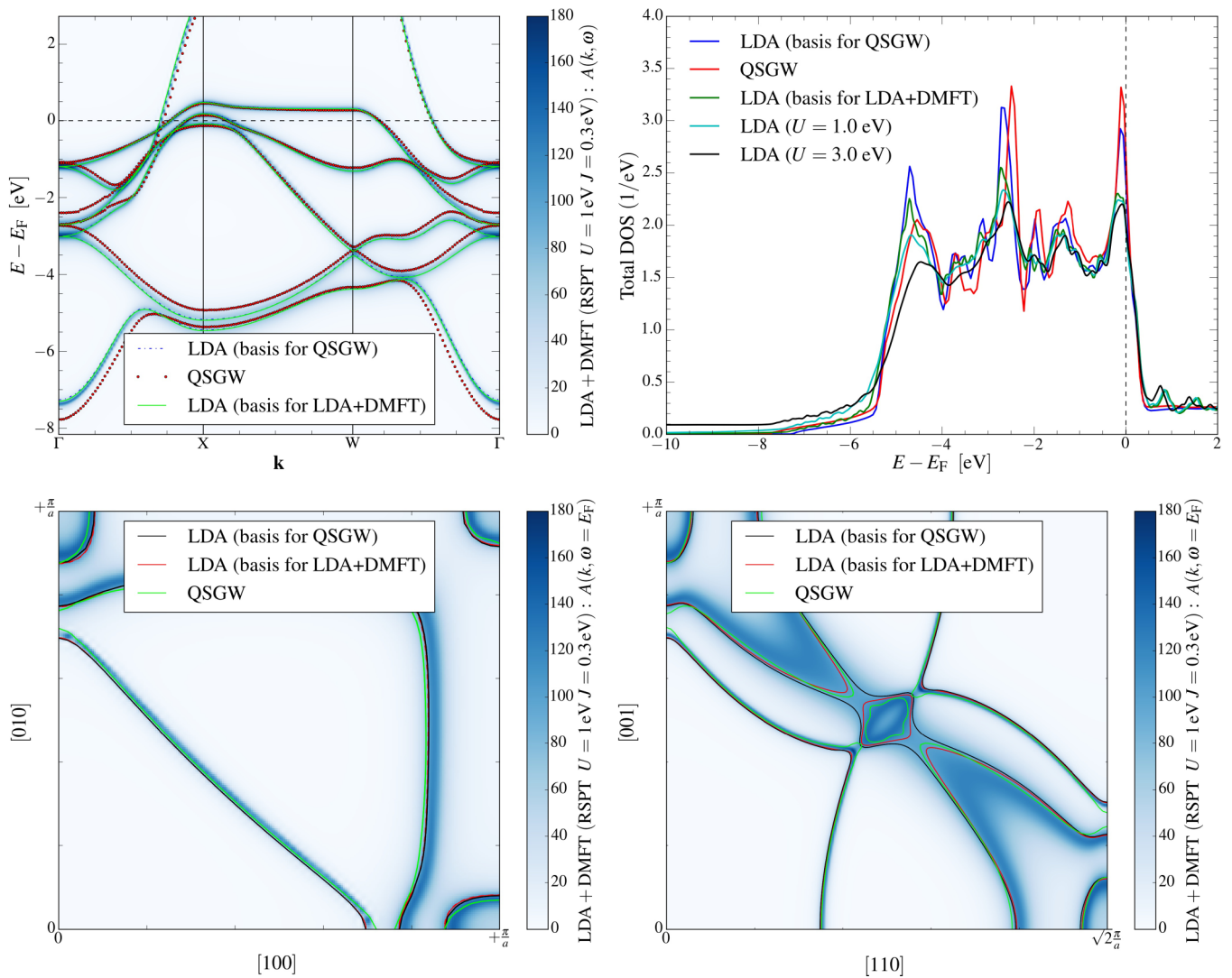
FIG. 6. Blue color map corresponds to LDA+DMFT, $U = 1.0$ eV, and $J = 0.3$ eV. Top left: Band structure along high-symmetry directions in the BZ. Top right: QSGW and LDA+DMFT DOS. Bottom left: Fermi surface cut in the k_x-k_y plane. Bottom right: Fermi surface cut including the L point.

The density of states calculated within the QSGW method (red line) and within LDA (blue line) are also plotted in Fig. 6 (top right). The effect of correlations is most easily identified by inspecting the three main peaks in the DOS. In Fig. 6 (top right), we also show the LDA+DMFT **k**-integrated spectral function. The spectral functions within LDA+DMFT are calculated along a horizontal complex contour at a distance δ from the real axis, giving a broadening to the DOS. We performed LDA density of states calculations within RSPt along the real axis as well, and found excellent agreement with the LDA from QSGW (not shown). As correlations are turned on, similar trends in the three main peaks can be observed for the QSGW method as within the LDA+DMFT method. One main difference, however, is that LDA+DMFT can produce the high-energy satellite, while QSGW cannot. This can be attributed to the T-matrix ladder diagrams which are present in the LDA+DMFT self-energy, but not in the QSGW self-energy. There exist extensions of the GW formalism that allow for T-matrix diagrams (see Refs. [81,82]) that are not included in the present study.

The computed Fermi surface in a cut of the k_x-k_y plane from both LDA+DMFT and QSGW is presented in Fig. 6 (bottom left). Both methods change the Fermi surface slightly. The topology of the sheets is unchanged, but the **k**-space volume enclosed by the sheets shows some effect of correlations. The largest changes can be seen in the tube structure running along the X-W-X symmetry directions. In the case of LDA+DMFT (blue intensity scale) the tube radius is slightly reduced, while for QSGW (green line) the radius is slightly increased. A different cut in the BZ, including the L pocket, is shown in Fig. 6 (bottom right). QSGW and LDA+DMFT display similar trends in the change of the Fermi surface, mainly the beginning of a "neck" formation in the Γ-L direction and a decreasing of the L-pocket diameter. Note that within the LDA solution used as a starting point for the QSGW, the L pocket and the "tongue" feature are connected along the X-L-X direction. We found by explicit calculation that this was attributed to the use of the tetrahedron **k**-point integration method, which pushes the hole sheet slightly upwards in energy, creating the connection.

To conclude this section, we note that nonlocal effects captured by the QSGW method on the spectral functions come close to our LDA+DMFT data.

IV. CONCLUSION

Electron correlations are commonly assumed to affect the electronic structure of the $3d$ elements to a larger degree than in the $4d$ elements due, in part, to the difference in d-state bandwidth. By electronic structure calculations within a LDA+DMFT context, we could show that, even though the LDA can provide a reasonable description of the electronic structure of Pd, correlation effects give important contributions to ground-state and spectral properties. We could improve the equilibrium lattice constant and bulk modulus from that of the LDA, and on expansion of the lattice constant Pd was shown to be ferromagnetic with a magnetic moment suppressed by spin fluctuations. The spectral function calculated with LDA+DMFT supported a formation of a satellite in the high-energy binding region while at the same time improving the band positions in comparison with experiment. The spectral function and the Fermi surface showed no major difference between the LDA+DMFT and QSGW method, and in particular the nesting vector in the $[\xi\xi0]$ direction was only slightly changed from its LDA value.

We found that the different Coulomb interaction parameters are required in order to reproduce the experimental equilibrium lattice constant on the one hand and the PES satellite on the other hand. The obtained values, however, fall in the range 1.5–4 eV of the recent constraint RPA calculations of Ref. [52], where different degrees of screening are considered. A possible origin of the observed discrepancies might lie in the ignored nonlocal correlations or the frequency dependence of U [52,83].

Within the present LDA+DMFT calculations the spin-fluctuation effects were shown to influence the volume at which the magnetic transition occurs, pushing it to a higher value than the LDA one. These results suggests that spin fluctuations could be important also for the case of low-dimensional systems, like surfaces, nanoparticles, or epitaxial thin films of Pd.

Our study confirms the band narrowing and favors the satellite formation picture reported in some experimental studies of Pd [17]. Previously, the difference between the PES and band-structure calculations has been attributed to surface effects [70], but our results indicate that correlations should be also taken into account. This goes along with the empirical arguments presented in the earlier studies [18,21]. The LDA+DMFT method should be able to probe the effect of correlations on the PES on an *ab initio* level, and further studies in conjunction with bulk and surface-sensitive PES should hopefully make it possible to disentangle surface and correlation effects from each other.

By performing *GW* calculations in combination with DMFT, the so-called GW+DMFT schema [83], nonlocal correlations and spin fluctuation can be captured on an equal footing, which turns out to be the next essential step for the realistic description of the physical properties of palladium. Particularly interesting in this context would be momentum-dependent susceptibilities that correctly address paramagnon physics, recently observed in the experimental studies of palladium [84].

[1] W. Metzner and D. Vollhardt, Phys. Rev. Lett. **62**, 324 (1989).

[2] A. Georges, G. Kotliar, W. Krauth, and M. J. Rozenberg, Rev. Mod. Phys. **68**, 13 (1996).

[3] G. Kotliar and D. Vollhardt, Phys. Today **57**, 53 (2004).

[4] G. Kotliar, S. Y. Savrasov, K. Haule, V. S. Oudovenko, O. Parcollet, and C. A. Marianetti, Rev. Mod. Phys. **78**, 865 (2006).

[5] K. Held, Adv. Phys. **56**, 829 (2007).

[6] J. Minar, H. Ebert, C. DeNadai, N. B. Brookes, F. Venturini, G. Ghiringhelli, L. Chioncel, M. I. Katsnelson, and A. I. Lichtenstein, Phys. Rev. Lett. **95**, 166401 (2005).

[7] J. Minar, J. Phys.: Condens. Matter **23**, 253201 (2011).

[8] P. Aebi, T. J. Kreutz, J. Osterwalder, R. Fasel, P. Schwaller, and L. Schlapbach, Phys. Rev. Lett. **76**, 1150 (1996).

[9] C. M. Schneider, U. Pracht, W. Kuch, A. Chassé, and J. Kirschner, Phys. Rev. B **54**, R15618 (1996).

[10] J. Braun, J. Minár, H. Ebert, A. Chainani, J. Miyawaki, Y. Takata, M. Taguchi, M. Oura, and S. Shin, Phys. Rev. B **85**, 165105 (2012).

[11] J. Sánchez-Barriga, J. Braun, J. Minár, I. Di Marco, A. Varykhalov, O. Rader, V. Boni, V. Bellini, F. Manghi, H. Ebert *et al.*, Phys. Rev. B **85**, 205109 (2012).

[12] A. I. Lichtenstein, M. I. Katsnelson, and G. Kotliar, Phys. Rev. Lett. **87**, 067205 (2001).

[13] F. J. Himpsel, J. A. Knapp, and D. E. Eastman, Phys. Rev. B **19**, 2919 (1979).

[14] A. Grechnev, I. Di Marco, M. I. Katsnelson, A. I. Lichtenstein, J. Wills, and O. Eriksson, Phys. Rev. B **76**, 035107 (2007).

[15] G. Chouteau, R. Fourneaux, K. Gobrecht, and R. Tournier, Phys. Rev. Lett. **20**, 193 (1968).

[16] V. L. Moruzzi and P. M. Marcus, Phys. Rev. B **39**, 471 (1989).

[17] D. Chandesris, G. Krill, G. Maire, J. Lecante, and Y. Petroff, Solid State Commun. **37**, 187 (1981).

[18] P. O. Nilsson, C. G. Larsson, and W. Eberhardt, Phys. Rev. B **24**, 1739 (1981).

[19] A. Liebsch, Phys. Rev. Lett. **43**, 1431 (1979).

[20] A. Liebsch, Phys. Rev. B **23**, 5203 (1981).

[21] N. Maartensson and B. Johansson, Phys. Rev. Lett. **45**, 482 (1980).

[22] W. Kohn, Phys. Rev. Lett. **2**, 393 (1959).

[23] D. A. Stewart, New J. Phys. **10**, 043025 (2008).

[24] Z.-L. Liu, J.-H. Yang, L.-C. Cai, F.-Q. Jing, and D. Alfè, Phys. Rev. B **83**, 144113 (2011).

[25] T. Y. Hsiang, J. W. Reister, H. Weinstock, G. W. Crabtree, and J. J. Vuillemin, Phys. Rev. Lett. **47**, 523 (1981).

[26] S. Doniach and S. Engelsberg, Phys. Rev. Lett. **17**, 750 (1966).

[27] N. F. Berk and J. R. Schrieffer, Phys. Rev. Lett. **17**, 433 (1966).

[28] M. T. Béal-Monod, S.-K. Ma, and D. R. Fredkin, Phys. Rev. Lett. **20**, 929 (1968).

[29] M. T. Béal-Monod and J. M. Lawrence, Phys. Rev. B **21**, 5400 (1980).

[30] W. Joss, L. N. Hall, G. W. Crabtree, and J. J. Vuillemin, Phys. Rev. B **30**, 5637 (1984).

[31] W. Joss and G. W. Crabtree, Phys. Rev. B **30**, 5646 (1984).

[32] W. F. Brinkman and S. Engelsberg, Phys. Rev. **169**, 417 (1968).

[33] P. Hertel, J. Appel, and D. Fay, Phys. Rev. B **22**, 534 (1980).

[34] T. Moriya, *Spin Fluctuations in Itinerant Electron Magnetism* (Springer, Berlin, 1985).

[35] P. Larson, I. I. Mazin, and D. J. Singh, Phys. Rev. B **69**, 064429 (2004).

[36] L. Hedin, Phys. Rev. **139**, A796 (1965).

[37] J. M. Wills, M. Alouani, P. Andersson, A. Delin, O. Eriksson, and O. Grechnyev, *Full-Potential Electronic Structure Method* (Springer-Verlag, Berlin, 2010).

[38] I. Di Marco, J. Minár, S. Chadov, M. I. Katsnelson, H. Ebert, and A. I. Lichtenstein, Phys. Rev. B **79**, 115111 (2009).

[39] O. Granas, I. di Marco, P. Thunström, L. Nordström, O. Eriksson, T. Björkman, and J. Wills, Comput. Mater. Sci. **55**, 295 (2012).

[40] M. van Schilfgaarde, T. Kotani, and S. Faleev, Phys. Rev. Lett. **96**, 226402 (2006).

[41] T. Kotani, M. van Schilfgaarde, and S. V. Faleev, Phys. Rev. B **76**, 165106 (2007).

[42] M. Imada, A. Fujimori, and Y. Tokura, Rev. Mod. Phys. **70**, 1039 (1998).

[43] A. G. Petukhov, I. I. Mazin, L. Chioncel, and A. I. Lichtenstein, Phys. Rev. B **67**, 153106 (2003).

[44] N. E. Bickers and D. J. Scalapino, Ann. Phys. (N.Y.) **193**, 206 (1989).

[45] A. I. Lichtenstein and M. I. Katsnelson, Phys. Rev. B **57**, 6884 (1998).

[46] M. I. Katsnelson and A. I. Lichtenstein, J. Phys.: Condens. Matter **11**, 1037 (1999).

[47] L. V. Pourovskii, M. I. Katsnelson, and A. I. Lichtenstein, Phys. Rev. B **72**, 115106 (2005).

[48] V. Drchal, V. Janis, J. Kudrnovsky, V. S. Oudovenko, X. Dai, K. Haule, and G. Kotliar, J. Phys.: Condens. Matter **17**, 61 (2005).

[49] J. P. Perdew and Y. Wang, Phys. Rev. B **45**, 13244 (1992).

[50] H. J. Vidberg and J. W. Serene, J. Low Temp. Phys. **29**, 179 (1977).

[51] M. Methfessel, M. van Schilfgaarde, and R. A. Casali, in *Electronic Structure and Physical Properties of Solids: The Uses of the LMTO Method*, edited by H. Dreysse (Springer-Verlag, Berlin, 2000).

[52] E. Şaşıoğlu, C. Friedrich, and S. Blügel, Phys. Rev. B **83**, 121101 (2011).

[53] A. P. Miiller and B. N. Brockhouse, Can. J. Phys. **49**, 704 (1971).

[54] C. N. Rao and K. K. Rao, Can. J. Phys. **42**, 1336 (1964).

[55] V. N. Staroverov, G. E. Scuseria, J. Tao, and J. P. Perdew, Phys. Rev. B **69**, 075102 (2004).

[56] D. A. Young, *Phase Diagrams of the Elements* (University of California Press, Berkeley, CA, 1991).

[57] S. S. Alexandre, M. Mattesini, J. M. Soler, and F. Yndurain, Phys. Rev. Lett. **96**, 079701 (2006).

[58] P. Mohn, *Magnetism in the Solid State* (Springer-Verlag, Berlin, 2002).

[59] B. Sampedro, P. Crespo, A. Hernando, R. Litrán, J. C. Sánchez López, C. López Cartes, A. Fernandez, J. Ramírez, J. González Calbet, and M. Vallet, Phys. Rev. Lett. **91**, 237203 (2003).

[60] A. Delin, E. Tosatti, and R. Weht, Phys. Rev. Lett. **92**, 057201 (2004).

[61] L. Vitos, B. Johansson, and J. Kollár, Phys. Rev. B **62**, R11957 (2000).

[62] S. Sakuragi, T. Sakai, S. Urata, S. Aihara, A. Shinto, H. Kageshima, M. Sawada, H. Namatame, M. Taniguchi, and T. Sato, Phys. Rev. B **90**, 054411 (2014).

[63] L. Fritsche, J. Noffke, and H. Eckardt, J. Phys. F: Met. Phys. **17**, 943 (1987).

[64] H. Chen, N. E. Brener, and J. Callaway, Phys. Rev. B **40**, 1443 (1989).

[65] S. C. Hong and J. I. Lee, J. Korean Phys. Soc. **52**, 1099 (2008).

[66] O. K. Andersen, Phys. Rev. B **2**, 883 (1970).

[67] H. Hayashi, K. Shimada, J. Jiang, H. Iwasawa, Y. Aiura, T. Oguchi, H. Namatame, and M. Taniguchi, Phys. Rev. B **87**, 035140 (2013).

[68] S. Y. Savrasov and D. Y. Savrasov, Phys. Rev. B **54**, 16487 (1996).

[69] F. J. Pinski, P. B. Allen, and W. H. Butler, Phys. Rev. Lett. **41**, 431 (1978).

[70] J.-S. Kang, D. W. Hwang, C. G. Olson, S. J. Youn, K.-C. Kang, and B. I. Min, Phys. Rev. B **56**, 10605 (1997).

[71] D. R. Lloyd, C. M. Quinn, and N. V. Richardson, Surf. Sci. **63**, 174 (1977).

[72] F. J. Himpsel and D. E. Eastman, Phys. Rev. B **18**, 5236 (1978).

[73] K. Yagi, K. Higashiyama, S. Yamazaki, H. Yanashima, H. Ohnuki, H. Fukutani, and H. Kato, Surf. Sci. **231**, 397 (1990).

[74] S. Hüfner, *Photoelectron Spectroscopy, Principles and Applications* (Springer-Verlag, Berlin, 2003).

[75] M. I. Katsnelson and A. I. Lichtenstein, Eur. Phys. J. B **30**, 9 (2002).

[76] F. M. Mueller, A. J. Freeman, J. O. Dimmock, and A. M. Furdyna, Phys. Rev. B **1**, 4617 (1970).

[77] D. H. Dye, S. A. Campbell, G. W. Crabtree, J. B. Ketterson, N. B. Sandesara, and J. J. Vuillemin, Phys. Rev. B **23**, 462 (1981).

[78] A. Kokalj, Comput. Mater. Sci. **28**, 155 (2003).

[79] C. R. Brown, J. P. Kalejs, F. D. Manchester, and J. M. Perz, Phys. Rev. B **6**, 4458 (1972).

[80] J. Kanamori, Prog. Theor. Phys. **30**, 275 (1963).

[81] V. P. Zhukov, E. V. Chulkov, and P. M. Echenique, Phys. Rev. B **72**, 155109 (2005).

[82] P. Romaniello, F. Bechstedt, and L. Reining, Phys. Rev. B **85**, 155131 (2012).

[83] P. Werner, M. Casula, T. Miyake, F. Aryasetiawan, A. J. Millis, and S. Biermann, Nat. Phys. **8**, 331 (2012).

[84] R. Doubble, S. M. Hayden, P. Dai, H. A. Mook, J. R. Thompson, and C. D. Frost, Phys. Rev. Lett. **105**, 027207 (2010).